Journal of Alloys and Compounds 509 (2011) 21–26

Contents lists available at ScienceDirect

Journal of Alloys and Compounds

journal homepage: www.elsevier.com/locate/jallcom

Sb effect on micro structural and mechanical properties of rapidly solidified Al–12Si alloy

O. Uzun, F. Yılmaz*, U. Kölemen, N. Başman

Gaziosmanpaşa University, Faculty of Arts and Sciences, Department of Physics, 60240 Tokat, Turkey

ARTICLE INFO

Article history:
Received 11 February 2010
Received in revised form 27 August 2010
Accepted 6 September 2010
Available online 16 September 2010

Keywords:
Rapid solidification
Al–Si alloy
Sb effect
Microstructure
Mechanical properties

ABSTRACT

The effects of antimony (Sb) addition on the microstructure and mechanical properties of rapidly solidified eutectic Al–Si alloy were investigated. Al–12 wt.%Si–*X* wt.%Sb (*X* = 0, 0.5 and 1.0) alloys were fabricated using a melt-spinner at rotating speeds of 20 m/s. The as-melt-spun ribbons were characterized by a combination of scanning electron microscopy (SEM), X-ray diffraction (XRD) and depth-sensing indentation (DSI) methods. SEM observations showed that 0.5%Sb addition refined the microstructure whereas 1.0%Sb addition led to the formation of coarse Si particles. The wheel side of the ribbons exhibited a finer microstructure than those on the free or air sides exposed to the atmosphere. According to the XRD results, the diffraction patterns of melt-spun ribbons consisted solely of α-Al and Si phases, and a possible volume fraction of AlSb or an intermetallic phase in the alloy was not observed. DSI tests were performed on the ribbons under different loads ranging from 200 to 1200 mN at room temperature. The resulting indentation load-displacement (*P–h*) curves were analyzed using the work of indentation approach (WIA) to evaluate the ribbons' microhardness (*H*) and reduced modulus (*Er*). We found that the *H* and *Er* values of the ribbon decrease with increasing Sb content. This can be attributed to the over modification and changes in the microstructure of Al–12%Si alloy when a minimum of 1.0%Sb is present as a modifier.

1. Introduction

Al–Si alloys are known as typical high-strength, corrosion resistant, and light-weight cast materials, and they are widely used for automobile and aerospace engines [1–3]. The excellent mechanical properties of these alloys are attributed to hard Si particles embedded in an Al-matrix. It is known that the size and shape of silicon particles in Al–Si alloy determine the mechanical properties of these alloys. Plate-like Si particles deteriorate the mechanical properties of the alloy, but fine and/or fibrous forms of Si particles enhance them. Fine and/or fibrous Si particles can be produced in various ways, such as by adding impurity elements [4–7], ternary alloying [8–10], and different casting techniques [6,7]. Many researchers have used sand and chill casting techniques [4–7,11]. In these techniques, cooling rate is limited. Si particles therefore cannot be refined sufficiently. Rapid solidification processes (RSP) have been the solution to this problem since Duwez et al. introduced the first RSP technique in 1960 [12]. Melt-spinning (MS) is an RSP technique with a higher cooling rate (10^5–10^7 K/s) than others methods [1,13,14]. Adding impurity elements (Ba, Ca, Mg, Na, Ni, P, Sb, Sr, Ti, Y, Yb), also called modifiers, to the Al–Si alloys is another method to refine the shape and size of silicon particles [4,5,7–10]. Among these, Na [7,9] and Sr [5,7,15] are the most widely used commercial modifiers. These convert the coarse eutectic Si into a fibrous eutectic structure very efficiently. However, they have numerous drawbacks. For example, they burn out from the melt easily because of their gassing tendency. Therefore, it is difficult to prepare the desired composition. They usually react with crucible. These modifiers also increase the hydrogen solubility in the alloys. This causes porosity and leads to the bad mechanical properties of alloys. Compared with Na and Sr, the addition of Sb does not result in a fibrous silicon structure but in a lamellar structure that is intermediate between acicular and fibrous. However, it has been reported that Sb can effectively refine the Al–Si eutectic structure providing a low susceptibility to gassing and excellent casting properties. For this reason, Sb has been used as an alternative to Na and Sr in the production of Al–Si alloys.

A wide range of practical applications requires knowledge of the mechanical properties of materials. Indentation hardness testing is a common technique for investigating the mechanical properties of materials. Depth-sensing indentation (DSI) is preferable to conventional hardness tests as it offers several advantages [16–19]. Apart from conventional hardness tests, the method is capable of measuring not only hardness (*H*) but also reduced elastic modulus (*Er*) of the materials. Furthermore, the load and displacement (depth) of an indentation are continuously monitored and optical

* Corresponding author. Tel.: +90 356 252 1616; fax: +90 356 252 1585..
E-mail address: fyilmaz@gop.edu.tr (F. Yılmaz).

0925-8388/$ – see front matter © 2010 Elsevier B.V. All rights reserved.
doi:10.1016/j.jallcom.2010.09.037

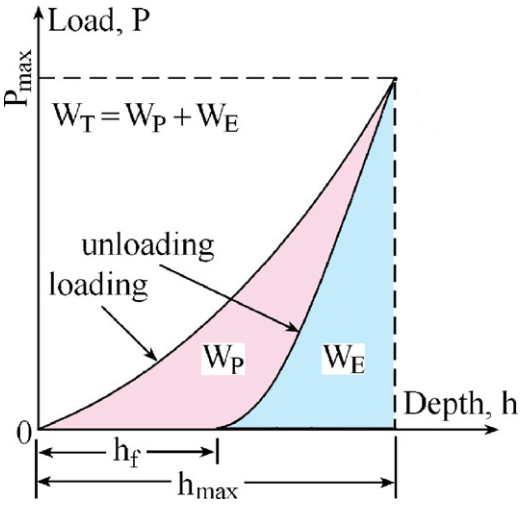

Fig. 1. Representative *P*–*h* curve.

observation and measurement of the diagonal length of the residual impression, which can be difficult and subjected to inaccuracy, are no longer required. Several analytical approaches have been developed to obtain mechanical properties from indentation load-displacement curve. Oliver and Pharr method (OP) and work of indentation approach (WIA) are widely adopted by researchers in order to calculate the hardness and reduced elastic modulus of the test materials [20–25]. A significant advantage of WIA is that, unlike OP, it takes the entire *P*–*h* curve into consideration, not only a part of the initial unloading curve. Additionally, this method reduces errors due to pile-up or sink-in behaviors observed around the indents. [24,25]. In the present study, we therefore prefer the *WIA* in calculations. The calculations are based on the integral of the loading and unloading curves. The area under the loading curve gives the total work (W_T) done during indentation, while the elastic contribution, W_E is given by the area under the unloading curve (Fig. 1). Thus, the plastic work W_P is the difference between W_T and W_E:

$$W_P = W_T - W_E = \int_0^{h_{max}} P(h)\,dh - \int_{h_f}^{h_{max}} P(h)\,dh \quad (1)$$

where P is the indentation load as a function of penetration depth (h), h_{max} is the maximum penetration depth, and h_f is the final unloading depth. It is known that in the literature [24] hardness can be calculated on the basis of the plastic work of indentation alone and can be represented by

$$H = \frac{\chi {P_m}^3}{9{W_P}^2} \quad (2)$$

where P_m is the peak indentation load and χ is a constant equal to 0.0378 for the Vickers indenter. Otherwise, regarding the work of indentation approach, reduced elastic modulus can be determined by the following equation [26,27]

$$\frac{W_E}{W_T} = 5\left(\frac{H}{E}\right) \quad (3)$$

To the best of our knowledge, there is no report on the combined effect of Sb modification and high cooling rate treatment on the mechanical properties of Al–12Si alloys. In the present work, we therefore aimed to investigate how Sb addition, together with high cooling rate treatments, affects the micro structural and mechanical properties of eutectic Al–12Si alloys.

Table 1
Chemical composition (wt.%) and sample codes of alloys.

Sample code	Composition (wt.%)	Surface
W0	Al–12Si	Wheel side
A0	Al–12Si	Air side
W0.5	Al–12Si-0.5Sb	Wheel side
A0.5	Al–12Si-0.5Sb	Air side
W1.0	Al–12Si-1.0Sb	Wheel side
A1.0	Al–12Si-1.0Sb	Air side

2. Experimental

Elemental Al (99.9% purity), Si (99.999% purity) and Sb (99.999 wt.% purity) were used to prepare the alloy of nominal composition Al–12%Si–*X*%Sb (*X* = 0, 0.5 and 1.0 and all percentages are wt.% unless otherwise stated). The master alloys were first produced in an induction heating smelter. Then the rapidly solidified counterparts of the master alloys were obtained using an Edmund Bühler SC melt-spinner apparatus where molten alloy in a boron–nitride crucible was ejected onto a polished copper wheel rotating at 20 m/s by pressurized argon of 250 mbar. All the manufacturing processes were undertaken in an argon atmosphere. The resulting melt-spun ribbons were typically ~90 μm in thickness and 1 cm in width. The capital W and A letters denote the wheel side and free or air side of ribbons, respectively. The numbers 0, 0.5 and 1.0 following the capitals denote the amount of wt.%Sb in the Al–12Si alloy (Table 1).

The wheel and opposing or air side of the ribbons were selected for the indentation test. Prior to the indentation test, damage on the surface was removed mechanically by grinding with 4000 grit and then polishing on 3, 1, and 0.25 μm diamond lap wheels. Indentation experiments were conducted with a depth-sensing indentation (DSI) instrument with a Vickers tip (Shimadzu, DUH-W201S) and load and displacement resolutions of ±19.6 μN and ± 1 nm, respectively. All tests were performed under the same operating conditions. For an easier interpretation of the material behavior at various depths, only the maximum load was changed at regular intervals; 200, 400, 600, 800, 1000, and 1200 mN, where the loading rate was 23.4 mN/s at each peak load.

The microstructures and phase identification of melt-spun ribbons were examined with scanning electron microscopy (SEM) and X-ray diffractometry (XRD). Prior to the SEM observation, as-cast ribbons were etched with Keller's reagent. SEM analysis was performed using a LEO Evo 40VP instrument at an acceleration voltage of 15 kV after the samples were coated with a vacuum-deposited gold layer in order to enhance contrast. All micrographs were taken at the same magnification (10.00KX or 10,000X). The XRD examination was performed using a Rgaku D/Max-IIIC X-ray diffractometer and CuKα radiation with a wavelength of 0.154 nm. For phase identification, measurements were recorded for a wide range of diffraction angles (2θ) ranging from 20° to 100° with a scan rate of 0.02°/s at 36 kV and 26 mA.

3. Results and discussion

SEM micrographs of the melt-spun Al–12Si–*X*Sb (*X*= 0, 0.5 and 1.0) alloys are shown in Fig. 2. It is clearly seen from the figure that Si particles embedded in the Al-matrix exhibit reasonably distinct properties in size and shape. Fig. 2a shows the SEM micrographs of the Al–12Si alloy without addition of Sb (A0 and W0). The microstructure seen in Fig. 2a reveals coarse needles of eutectic silicon. Fig. 2b and c represent the microstructure of Al–12Si alloy inoculated with 0.5 (A0.5 and W0.5) and 1.0% Sb (A1.0 and W1.0), respectively. The melt-spun alloy with 0.5%Sb content produced finely branched microstructures on both surfaces (Fig. 2b). Acicular Si phase was completely absent and lamellar type structure turned to fully modified structure. The alloy with 1.0%Sb content shows similar morphology to that observed in the unmodified alloy, but with a slightly finer eutectic silicon needles. It is well known that Sb acts more likely as a eutectic silicon refining agent in Al–Si alloys and at concentration levels equal to or greater than 0.05%, Sb refines the eutectic Si phase [28]. Typical levels found in Sb treated alloys in the literature range from 0.05% to 0.8% depending on the composition of the alloy [6,7,29–32]. Accordingly, an optimum level of modifier is required to produce a given microstructure. A higher level than optimum concentration results in an over modified structure characterized by coarse microconstituents. In our case, the rather coarser microstructure observed in alloy for 1.0%Sb can be understood by the over modification effect of Sb. Similar results were obtained in the literature and these were attributed to a new

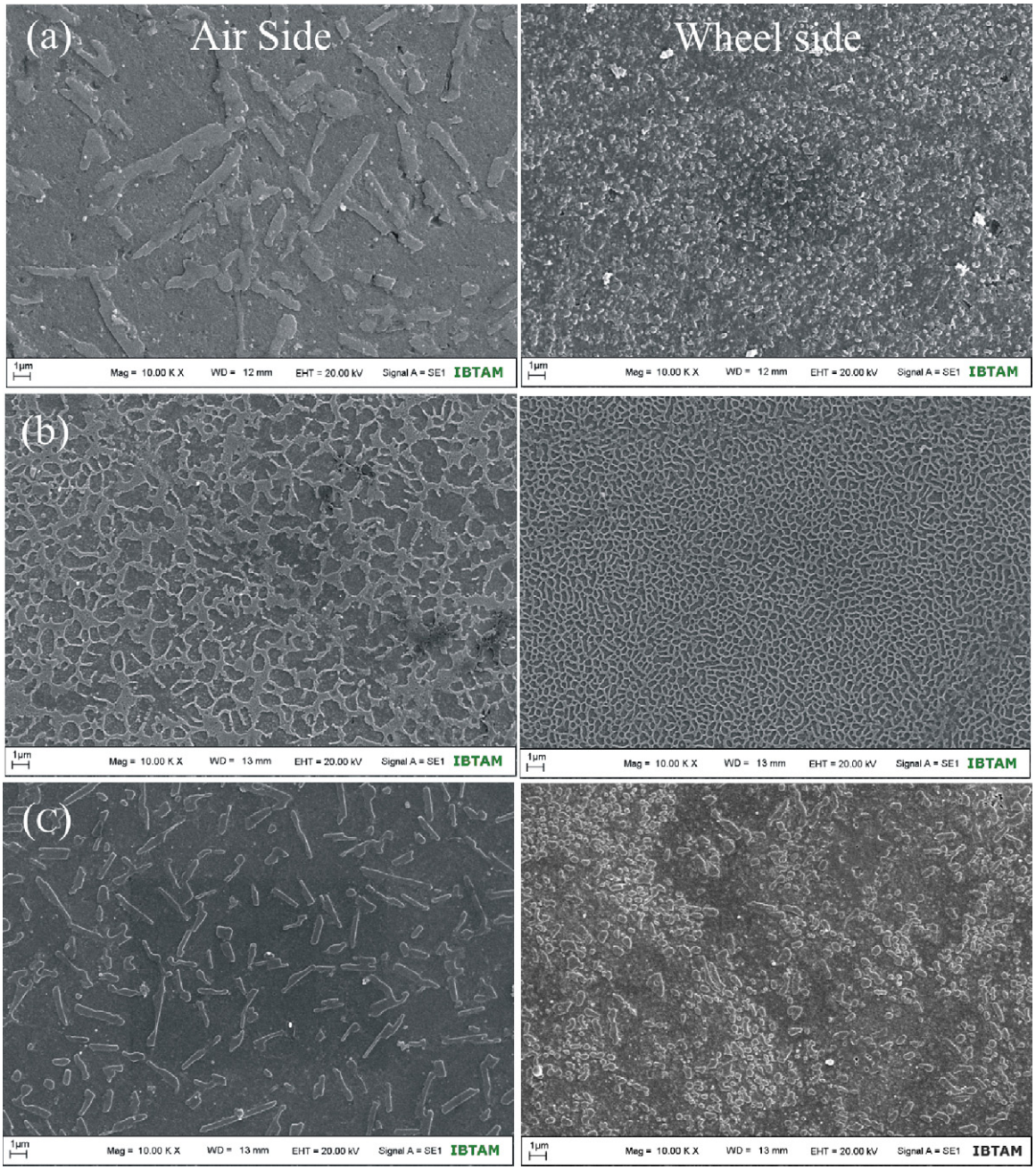

Fig. 2. SEM micrograph of air (left column) and wheel side (right column) of the melt-spun ribbons (a) A0 and W0, without Sb (b) A0.5 and W0.5, 0.5%Sb addition (c) A1.0 and W1.0, 1.0%Sb addition.

intermetallic phase (AlSb) formation in microstructure and promotion of Si aggregation [31–33]. In this research, although XRD patterns exhibit the α-Al and Si phase, they do not display the AlSb intermetallic phase on microstructures for all specimens (Fig. 3). It is well known that antimony has limited solid solubility in aluminium (<0.01%) in an equilibrium condition. AlSb intermetallic phase formation is highly expected due to its higher entropy of fusion when compared to metals. However, possible volume fraction of AlSb intermetallic phase in the alloy was not observed in both the SEM and XRD analyses. Non-observation of the AlSb micro constituent may be attributed to a minor deviation in quantity or a small volume fraction ($\leq$1%) of the AlSb intermetallic phase. On the other hand, Hegde and Probhu [33] reported that Sb addition promotes the aggregation of silicon, thus changing the shape and size of silicon in the solid state. Hence, the coarsening behavior of Si particles observed in microstructure for 1.0%Sb added Al–Si alloy (Fig. 2c and d), can be understood by the promotion of Si aggregations.

The microstructure of an individual melt-spun ribbon is somewhat variable from the wheel (or contact) side to the free (or air) side. The air surfaces of the ribbons have a relatively coarser and inhomogeneous microstructure when compared to their wheel side counterparts (Fig. 2). This micro structural coarsening tendency on the air surface can be attributed to a slower cooling rate. The stability of the solid-liquid interface decreases with the reduction of cooling rate on the air surface, and the structure becomes coarser. SEM cross-section micrograph of the unmodified alloy clearly reveals the micro structural variation of the ribbon (Fig. 4). The featureless zone on the wheel side is typical of rapidly solidified alloys and is a result of the extreme grain refinement due to the high cooling rates. Using the empirical relation proposed by Matyja

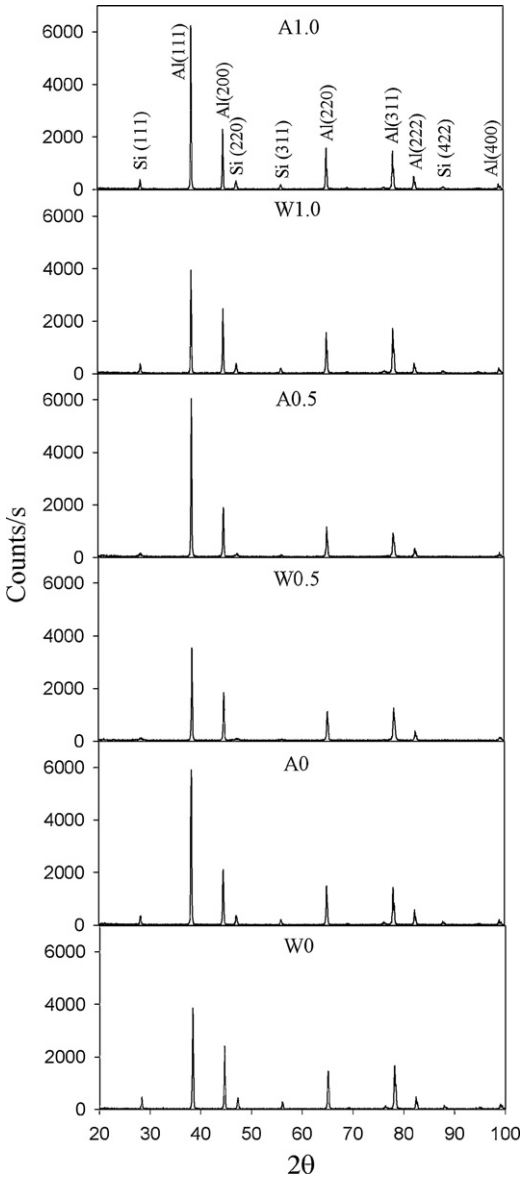

Fig. 3. XRD patterns of melt-spun ribbons having different Sb content.

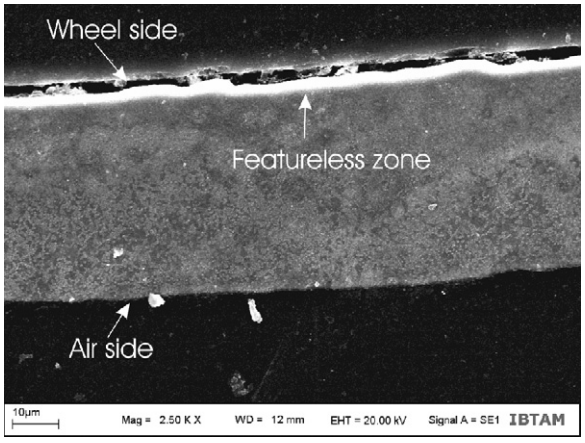

Fig. 4. Cross-section morphology of melt-spun Al–12Si (without Sb) ribbon.

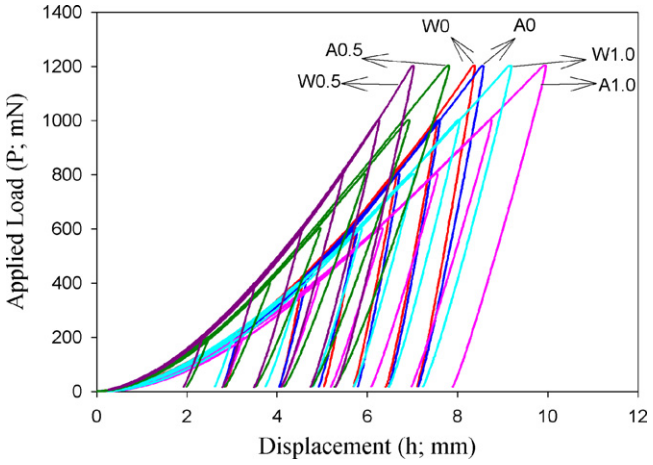

Fig. 5. Load-displacement curves of the samples.

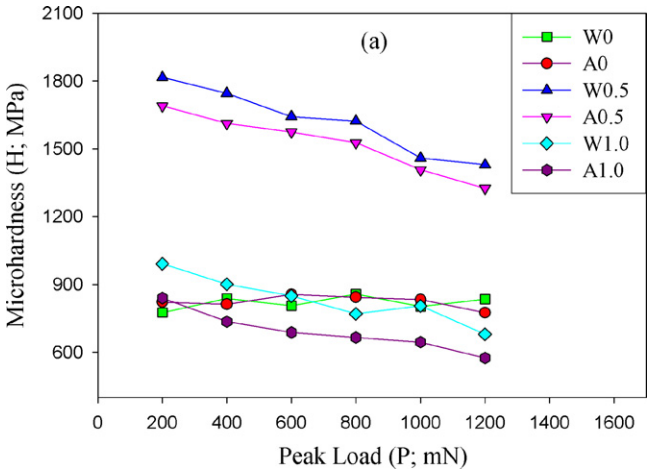

Fig. 6. Hardness variation as a function of peak loads.

et. al. [34] of $R = (47/d)^3$ for an Al–12Si–0.5Sb alloy (Fig. 2b), where d is the cell size (in μm) and R the cooling rate, the cooling rates were found to be $\sim 6 \times 10^4$ and $\sim 1.4 \times 10^5$ K/s for the air side and the wheel side, respectively.

Applied load–displacement (P–h) curves of the samples at different peak loads are shown in Fig. 5. The overlapping characteristic of the curves implies that all samples have a homogeneous structure. Shifting the unloading parts to a higher displacement indicates that indented material was subjected to further plastic deformation. As hardness is described as the resistance of material against permanent or plastic deformation, with regard to unloading, the hardness of the samples can be arranged as W0.5 > A0.5 > W0 > A0 > W1.0 > A1.0. However, for quantitative results, the curves must be analyzed in detail. In this study, the work of indentation approach was used for analyzing the curves. The hardness values calculated using Eq. (2) are given in Fig. 6 and Table 2. All values showed a load dependent behavior called the indentation size effect (ISE). This phenomenon was observed in previous studies and explained by a variety of causes such as work hardened surface layers, hard surface oxides, contaminants, tip bluntness or poor tip-shape calibrations, all of which could result in the ISE [35–37]. The most adopted model developed by Nix and Gao is based on a geometrically necessary dislocation occurring beneath a conical indenter [38]. The present authors also investigated ISE behavior in superconductors and rapidly solidified alloys [16–19]. It is well known that any defect in the regular crystal structure

Table 2
Hardness and Reduced elastic modulus values of the samples.

Peak load (mN)	Hardness (MPa)						Reduced elastic modulus (GPa)					
	W0	A0	W0.5	A0.5	W1.0	A1.0	W0	A0	W0.5	A0.5	W1.0	A1.0
200	776	823	1816	1690	992	840	32	29	49	44	21	16
400	839	813	1745	1612	901	736	28	24	40	38	17	11
600	807	856	1642	1574	850	688	25	22	35	35	15	10
800	858	844	1623	1526	770	665	23	23	35	32	13	9
1000	803	833	1458	1406	806	645	22	22	30	28	14	9
1200	836	775	1429	1324	680	575	21	19	28	26	11	8

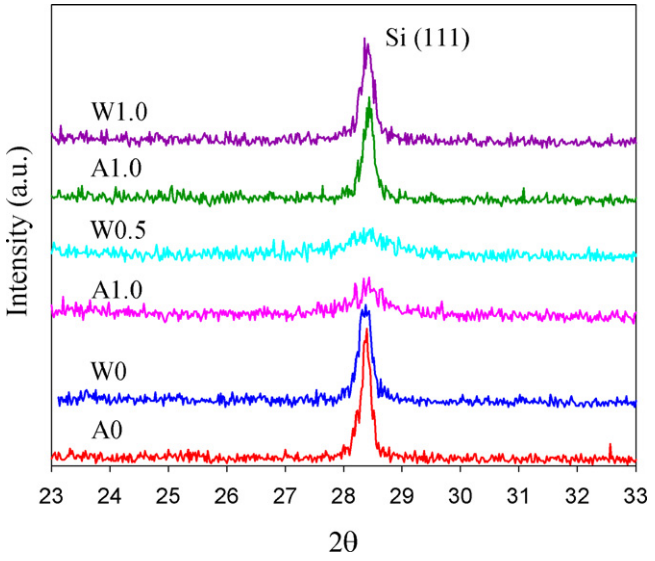

Fig. 7. The enlarged part of the XRD diffractogram in the angular range 23–33° showing Si (111) diffraction peak for the samples.

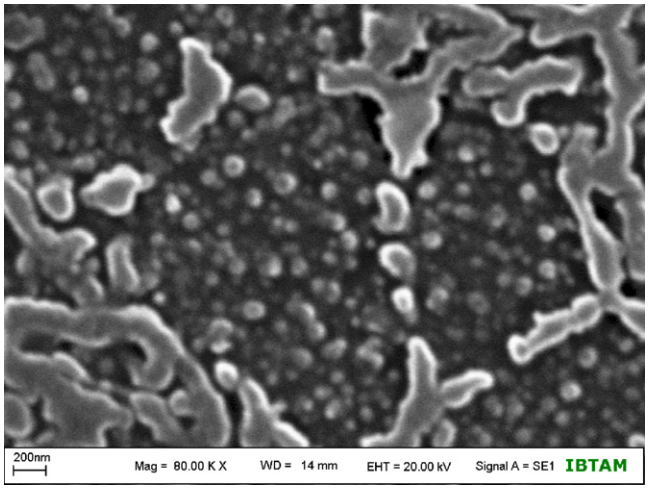

Fig. 8. The enlarged part of the SEM micrograph of W0.5 showing spherical Si nano-grains.

or grain boundaries obstructs the dislocation, which makes plastic deformation more difficult. This requires extra force to achieve the dislocation, or to strengthen the material. So, one can say that the greater the crystal defects or grain boundary density are, the greater are the hardness values. XRD peak broadening and decrease of its intensity are the results of ultra fine and even nano-grain formation. Fig. 7 shows the Si (1 1 1) diffraction peak for all samples. From the figure, it is clear that diffraction peak of W0.5 is broader and its relative intensity is smaller than that of other samples. Furthermore, SEM enlarged micrograph of W0.5 shows spherical Si nano-grains that are approximately 90–100 nm in dimension (Fig. 8). Accordingly, the highest H values obtained for W0.5 accords well with the above explanation. A1.0 has the lowest hardness values due to a lack of efficient grain boundary density. Crystallite size is another factor that affects mechanical properties of alloys. The crystallite size of as-melt-spun alloys was estimated using the Williamson–Hall method [39]. The Williamson–Hall equation is expressed as follows:

$$\beta \cos\theta = \frac{K\lambda}{D} + \varepsilon \sin\theta \quad (4)$$

where β is the full-width at half-maximum (FWHM) of the XRD peaks in radians, K is Scherrer constant ($K = 0.9$), D is the crystallite size, λ is the X-ray wavelength ($\lambda_{CuK\alpha 1} = 0.15406$ nm), ε is the lattice strain and θ is the Bragg angle. In this method, $\beta\cos\theta$ is plotted against $\sin\theta$. Using a linear extrapolation to this plot, the intercept gives the crystallite size $K\lambda/D$ and slope gives lattice strain (ε). Williamson–Hall plots of the present samples are shown in Fig. 9. The approximate sizes calculated from the graph are 244, 378, 107, 153, 190, 253 nm for the samples W0, A0, W0.5, A0.5, W1.0 and A1.0, respectively. According to the Hall–Petch relation, hardness is inversely proportional to the square root of crystallite size. As an agreement with Hall–Petch relation, we observed that the grain refinement has increased the hardness. Hence, high hardness of the W0.5 can be attributed to the smaller grain size. The grain refinement is also supported by the SEM examination As a conclusion, high hardness value of 0.5%Sb added sample may be explained by increase of the crystal defects and grain boundary density, decrease of the crystallite size and homogeneous distribution of Si phase. As discussed in SEM examination 1.0%Sb addition caused over modification.

The reduced elastic modulus values calculated using Eq. (3) are given in Fig. 10 and Table 2. All Er values are well below

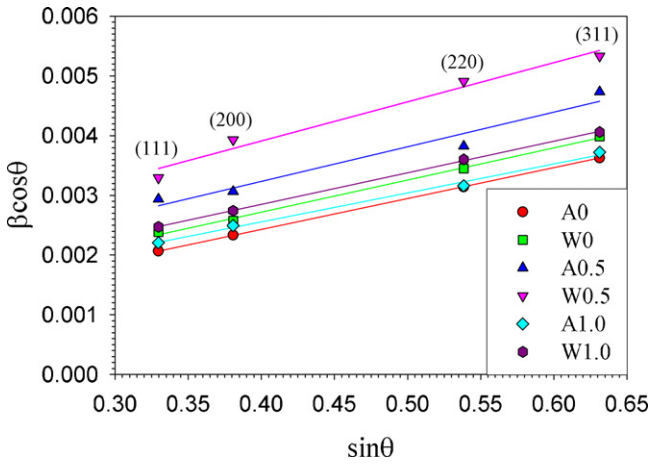

Fig. 9. Williamson–Hall plots showing X-ray peak broadening as function of Bragg angle for the samples (The four most intensive reflection peaks were used in the line broadening analysis).

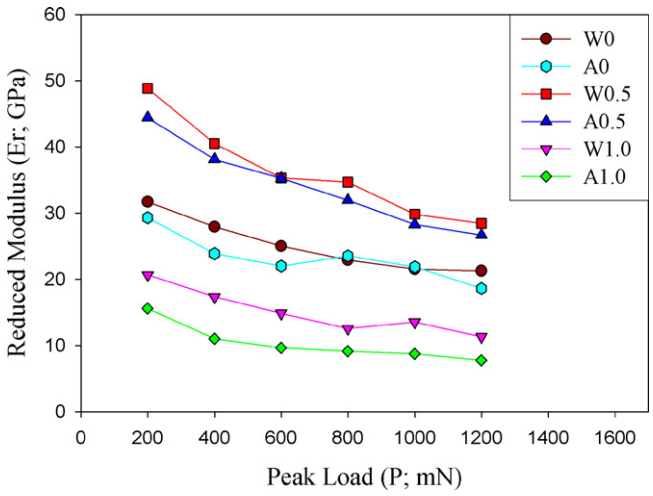

Fig. 10. Reduced elastic modulus variation as a function of peak loads.

the literature value of eutectic Al–Si alloy, 69 GPa [40]. Both RSP and Sb addition were responsible for the reduction of *Er* values. Nanocrystalline materials in general are found to exhibit significantly lower elastic modulus than their bulk counterparts, and increased porosity and volume fractions of grain boundaries and triple junctions are believed to be the reason [41]. This may be very useful in application areas that require flexibility. Differences in *Er* values between the samples can be explained using the similar approach applied to hardness mechanism. Likewise, it is expected that refinement of the crystallite size also enhances flexibility. Considering the approach, the *Er* values of the samples must range as W0.5 > A0.5 > W0 > A0 > W1.0 > A1.0. Present experimental data shows that the proposed approach is correct.

4. Conclusion

The changes in the microstructures and mechanical properties of Al–12%Si alloy modified with Sb were examined and following conclusions were obtained. Content of Sb (wt.%0.5) in the alloy was quite important to obtain fine microstructures that consist of fibrous Si particles. The larger Sb (wt.%1.0) content resulted in crystallization of Si atoms solved in Al-matrix and led to poor mechanical properties. It was also found that the mechanical properties of wheel side were more developed than that of air side due to the good heat extraction.

Acknowledgements

This work was supported by Turkish State Planning Organisation (DPT) (Project No: 2003K120510). The authors would like to acknowledge Eyüphan Yakıncı for SEM analysis and Cabir Terzioğlu for XRD analysis.

References

[1] M.L. Öveçoğlu, N. Ünlü, N. Eruslu, A. Genç, Mater. Lett. 57 (2003) 3296–3301.
[2] K. Matsuura, M. Kudoh, H. Kinoshita, H. Takahashi, Mater. Chem. Phys. 81 (2–3) (2003) 393–395.
[3] J. Zhou, J. Duszczyk, J. Mater. Sci. 25 (1990) 4541–4548.
[4] A. Knuutinen, K. Nogita, S.D. McDonald, A.K. Dahle, J. Light Met. 1 (2001) 229–240.
[5] B. Suarez, J. Asensio, Mater. Charact. 55 (4–5) (2006) 218–226.
[6] A. Ourdjini, R. Elliott, Mater. Sci. Tech. 11 (1995) 1241–1245.
[7] N. Fatahalla, M. Hafiz, M. Abdulkhalek, J. Mater. Sci. 34 (1999) 3555–3564.
[8] N.L. Tawfik, J. Mater. Sci. 32 (1997) 2997–3000.
[9] C.R. Ho, B. Cantor, J. Mater. Sci. 30 (1995) 1912–1920.
[10] N.L. Tawfik, E.M. Abdel Hady, N.E. Kassem, Mater. Trans. 30 (5) (1997) 401–405.
[11] Y. Hongkun, D. Zhang, T. Sakata, H. Mori, J. Alloy. Compd. 354 (1–2) (2003) 159–164.
[12] P. Duwez, R.H. Willens, W. Klement, J. Appl. Phys. 31 (6) (1960) 1136–1137.
[13] O. Uzun, T. Karaaslan, M. Gogebakan, M. Keskin, J. Alloy. Compd. 376 (2004) 149–157.
[14] M. Salehi, K. Dehghani, J. Alloy. Compd. 457 (1–2) (2008) 357–361.
[15] M. Van Rooyen, N.M. Van Der Pers, T.H.H. De Keijser, E.J. Mittemeijer, Mat. Sci. Eng. 96 (1987) 17–25.
[16] O. Şahin, O. Uzun, U. Kölemen, N. Uçar, Mater. Charact. 59 (2008) 729–736.
[17] U. Kölemen, O. Uzun, M.A. Aksan, N. Güçlü, E. Yakıncı, J. Alloy. Compd. 415 (1–2) (2006) 294–299.
[18] O. Uzun, U. Kölemen, S. Çelebi, N. Güçlü, J. Eur. Ceram. Soc. 25 (2005) 959–977.
[19] O. Uzun, T. Karaaslan, M. Keskin, J. Alloy. Compd. 358 (2003) 104–111.
[20] W.C. Oliver, G.M. Pharr, J. Mater. Res. 7 (6) (1992) 1564–1583.
[21] N.A. Stillwell, D. Tabor, Proc. Phys. Soc. Lond. 78 (2) (1961) 169–179.
[22] M. Sakai, Acta Metall. Mater. 41 (6) (1993) 1751–1758.
[23] M.T. Attaf, Mater. Lett. 57 (2003) 4684–4693.
[24] J.R. Tuck, A.M. Korsunsky, S.J. Bull, R.I. Davidson, Surf. Coat. Tech. 137 (2001) 217–224.
[25] D. Beegan, S. Chowdhury, M.T. Laugier, Surf. Coat. Tech. 192 (2005) 57–63.
[26] W.C. Oliver, G.M. Pharr, J. Mater. Res. 19 (1) (2004) 3–20.
[27] N.K. Mukhopadhyay, G.C. Weatherly, J.D. Embury, Mater. Sci. Eng. A 315 (1–2) (2001) 202–210.
[28] C. Comte, J. von Stebut, Surf. Coat. Tech. 154 (2002) 42–48.
[29] S. Boontein, J. Kajornchaiyakul, C. Limmaneevichitr, J. Mater. Sci. Technol. 24 (1) (2008) 25–28.
[30] B. Xiufang, W. Weimin, Q. Jingyu, Mater. Charact. 46 (2001) 25–29.
[31] A.K. Prasada Rao, K. Das, B.S. Murty, M. Chakraborty, Mater. Lett. 62 (2008) 2013–2016.
[32] F. Kahraman, M.K. Kulekci, SAÜ. Fen Bilimleri Dergisi 11 (1) (2007) 10–14.
[33] S. Hegde, K. Narayan Prabhu, J. Mater. Sci. 43 (2008) 3009–3027.
[34] H. Matyja, B.C. Giessen, N.J. Grang, J. Ins. Met. 96 (1968) 30.
[35] W.B. Li, R. Warren, Acta Metall. Mater. 42 (1993) 3065–3069.
[36] J.B. Pethica, D. Tabor, Surf. Sci. 89 (1979) 182–190.
[37] D.M. Turley, L.E. Samuels, Metallograpy 14 (1981) 275–294.
[38] W.D. Nix, H. Gao, J. Mech. Phys. Solids 46 (1998) 411–425.
[39] G.K. Williamson, W.H. Hall, Acta Metall. 1 (1953) 22–31.
[40] W. Soboyejo, Mechanical Properties of Engineered Materials, Marcel Dekker, New York, 2002.
[41] H. Li, A.H.W. Ngan, Scripta Mater. 52 (2005) 827–831.